This paper describes objective technical results and analysis. Any subjective views or opinions that might be expressed in the paper do not necessarily represent the views of the U.S. Department of Energy or the United States Government.

Combustion and Flame

SAND2019-8792J

Assessing an experimental approach for chemical explosive mode and heat release rate using DNS data

--Manuscript Draft--

Manuscript Number:	CNF-D-19-00294R3
Article Type:	Full Length Article
Keywords:	Raman/Rayleigh; heat release rate; chemical explosive mode; OH-LIF
Corresponding Author:	Sandra Hartl TU Darmstadt Darmstadt, GERMANY
First Author:	Sandra Hartl
Order of Authors:	Sandra Hartl
	Dirk Geyer
	Christian Hasse
	Xinyu Zhao
	Haiou Wang
	Robert S. Barlow
Abstract:	Obtaining information about burning characteristics and flame structures by analyzing experimental data is an important issue for understanding combustion processes and pursuing combustion modelling approaches. It has been shown that Raman/Rayleigh measurements of major species and temperature can be used to approximate the local heat release rate and the chemical explosive mode, and that these results are sufficiently accurate for a qualitative assessment of the relative importance of different heat release zones within the same overall flame structure in laminar and mildly turbulent partially premixed flames [1, 2]. The present study uses data from direct numerical simulation (DNS) to extend and quantify the understanding of the approximation method with respect to premixed and stratified-premixed flames with significant turbulence-chemistry interaction (high Karlovitz number). The accuracy of the approximation procedure is assessed as previously applied, using just major species and temperature, as well as with the OH radical included as an additional experimentally accessible species. The accuracy of the local chemical explosive mode and the local heat release rate results from the approximation are significantly improved with OH included, yielding quantitative agreement with the DNS results. Further, a global sensitivity analysis is applied to identify the sensitivity of the heat release rate and chemical explosive mode to experimental uncertainties imprinted upon the DNS data prior to the approximation procedure.

Sandia National Laboratories is a multimission laboratory managed and operated by National Technology & Engineering Solutions of Sandia, LLC, a wholly owned subsidiary of Honeywell International Inc., for the U.S. Department of Energy's National Nuclear Security Administration under contract DE-NA0003525.

Manuscript Click here to view linked References

Assessing an experimental approach for chemical explosive mode and heat release rate using DNS data

S. Hartl[a,b,*], D. Geyer[a], C. Hasse[b], X. Zhao[c], H. Wang[d], R. S. Barlow[e]

[a] Laboratory of Optical Diagnostics and Renewable Energies, University of Applied Sciences, Darmstadt, Germany
[b] FG Simulation of Reactive Thermo-Fluid Systems, TU Darmstadt, Darmstadt, Germany
[c] Department of Mechanical Engineering, University of Connecticut, Storrs, CT 06269, United States
[d] School of Photovoltaic and Renewable Energy Engineering, The University of New South Wales, NSW 2052, Australia
[e] Combustion Research Facility, Sandia National Laboratories, Livermore, USA

Abstract

Obtaining information about burning characteristics and flame structures by analyzing experimental data is an important issue for understanding combustion processes and pursuing combustion modelling approaches. It has been shown that Raman/Rayleigh measurements of major species and temperature can be used to approximate the local heat release rate and the chemical explosive mode, and that these results are sufficiently accurate for a qualitative assessment of the relative importance of different heat release zones within the same overall flame structure in laminar and mildly turbulent partially premixed flames [1, 2]. The present study uses data from direct numerical simulation (DNS) to extend and quantify the understanding of the approximation method with respect to premixed and stratified-premixed flames with significant turbulence-chemistry interaction (high Karlovitz number). The accuracy of the approximation procedure is assessed as previously applied, using just major species and temperature, as well as with the OH radical included as an additional experimentally accessible species. The accuracy of the local chemical explosive mode and the local heat release rate results from the approximation are significantly improved with OH included, yielding quantitative agreement with the DNS results. Further, a global sensitivity analysis is applied to identify the sensitivity of the heat release rate and chemical explosive mode to experimental uncertainties imprinted upon the DNS data prior to the approximation procedure.

Keywords: Raman/Rayleigh, heat release rate, chemical explosive mode, OH-LIF

1. Introduction

The heat release rate is one of the most fundamental local quantities which can be used to detect and characterize reaction zones in laminar and turbulent flames. However, assessing this quantity experimentally remains difficult [3, 4]. Several markers associated with the main chemical pathways for heat release have been proposed and evaluated through simulation [4-7], including HCO and the concentration products [CO]x[OH], [CH_2O]x[OH] or [CH_2O]x[H]. The most commonly applied experimental approach to provide information on heat release combines planar laser-induced fluorescence (PLIF) of formaldehyde and the hydroxyl radical, due to the relative simplicity of the techniques and strength of signals. While this approach has provided very useful data on the topology and relative strength of the main heat release regions, it is not a quantitative measure of the heat release rate.

Chemical explosive mode analysis is a computational flame diagnostic method to extract information from detailed chemistry simulations by analysing the eigenvalues of the chemical Jacobian [8]. Chemical explosive mode analysis has been successfully applied to direct numerical simulations [8-10] and under-resolved LES [10, 11] in order to, among other things, identify premixed reaction zones or auto-ignition fronts. While it is obvious that eigenvalues can be calculated from simulations, a method for approximating the chemical explosive mode starting from only temperature and major species concentrations was developed only recently [1].

The calculation of the chemical explosive mode and the heat release rate requires knowledge of the full thermochemical state, including minor species. In previous work it was demonstrated that knowledge of the local temperature and major species is sufficient to allow an approximation of the full thermochemical state by running a constrained homogeneous constant-pressure, constant-temperature reactor calculation using the Raman/Rayleigh accessible species (N_2, O_2, CH_4, CO_2, H_2O, CO, H_2) and temperature as initial state [1, 2]. The purpose of the homogeneous reactor calculation is to allow radicals and minor species to build up from zero initial values, such that the resulting approximation of the full thermochemical state remains consistent with the available experimental data. Accordingly, during the calculation, the seven major species are constrained to remain at their initial values or to remain within the bounds of the reported experimental uncertainties, depending on the specific implementation. The chemical explosive mode and the heat release rate are then calculated from this approximated full thermochemical state. The validity of this approach to obtain at least qualitative agreement was demonstrated in laminar and mildly turbulent partially premixed flames [1]. Further, the local heat release rate and the chemical explosive mode were used to

* Corresponding author:
S. Hartl
Full postal address: Otto-Berndt-Str. 2, 64287 Darmstadt, Germany
Email address: hartl@stfs.tu-darmstadt.de
Phone number: +49 6151 16-24153

interpret the relative importance of premixed and non-premixed reaction zones in partially premixed flames where both combustion regimes were present [2].

Recent experimental studies have been pushing towards high Karlovitz numbers, in an effort to observe and understand the broadened flame structures and frequent flame-flame interactions in turbulent premixed flames [12-15]. One burner was designed to produce turbulence intensity up to 30 % and integral scales much larger than the flame thickness [12, 14, 16]. In some cases, the flames are stratified due to mixing between the main jet fluid and combustion products of the large surrounding pilot flow [17, 18]. PLIF imaging of OH, CH_2O, and CH has been applied in these studies to visualize flame structures. Information on turbulent flame speed has been inferred through the measurements of flame surfaces that are defined based on the conventional species-based heat release rate markers, i.e., $[CH_2O]x[OH]$. As demonstrated in [4], the conventional heat release rate markers fail to capture the low-intensity heat release regions that are present downstream of the high Karlovitz number jet flames. With accumulated CO and H_2 molecules in the downstream locations, the slow oxidation reactions such as recombination of CO and OH can contribute 20% to 30% of the total heat release rates in that region.

In the present work, the homogeneous reactor approach for approximating the full thermochemical state is applied to data from direct numerical simulations (DNS) in order to extend and quantify our understanding of the validity of the method in application to turbulent flames with high Karlovitz number. Major species and temperature are taken from DNS of turbulent flames and are constrained to their original values in the homogeneous reactor calculation. Two recent DNS of turbulent methane-air premixed flames are used, which feature Karlovitz numbers up to 253, placing the flames in the thin reaction zone and broken flame regime, respectively. Both simulations employ a lean methane-air mixture at an equivalence ratio of 0.7 as the fuel inlet stream. With different levels of stratification, due to mixing between the reactant jet and the hot coflow, the two test cases feature an increasing impact of diffusive transport effects, which provides a hierarchical test to the method developed.

Additionally, the OH radical is considered as a scalar of interest. Preliminary analysis based on laminar flame calculations has shown that inclusion of OH in the input to the homogeneous reactor calculation leads, especially for high strain rates, to improved results for the chemical explosive mode and the heat release rate compared to the reference numerical results [1]. Therefore, a further motivation is to evaluate the benefits of adding OH as a known or quantitatively measured scalar in flames that have significant turbulence-chemistry interaction. Note that by combining OH-LIF with Raman/Rayleigh measurements of temperature and major species, it becomes possible to correct the OH signals on a shot-to-shot basis for changes in the local Boltzmann fraction and collisional quenching rate.

To further identify the sensitivity in the local heat release rate and chemical explosive mode, experimental uncertainties are imprinted in two different ways prior to the homogeneous reactor calculation. First, uncertainty quantification (UQ) tools are used to understand the sensitivity of the chemical explosive mode and the heat release rate to random experimental uncertainty in OH and major species in the context of this DNS. Second, experimental uncertainty in individual species (based on typical characteristics of Raman/Rayleigh systems in flames) is superimposed onto the numerical data.

The structure of the paper is as follows. Relevant flame markers are introduced in Section 2, and the conditions of the target flames are given in Section 3. The comparison of approximated and full results for the heat release rate and chemical explosive mode with no imposed uncertainty is made in Section 4, using fully resolved simulations of two highly turbulent flames. Further, the impact of including OH as an input to the homogeneous reactor calculation is quantified. In Section 5 the effects of experimental uncertainty are discussed based on UQ methods as well as a single species analysis focusing on specific influences. Conclusions are given in Section 6.

2. Flame markers

The quantities of interest (QoI) analyzed within this work - the mixture fraction, the chemical explosive mode, and the heat release rate - are briefly introduced in the following.

The mixture fraction is an essential parameter for characterizing inhomogeneous systems. Based on the Raman-accessible major species (N_2, O_2, CH_4, CO_2, H_2O, CO, H_2), the element-based Bilger mixture fraction Z [19] is defined as:

$$Z = \frac{\frac{2(Y_\mathrm{C} - Y_\mathrm{C,ox})}{W_\mathrm{C}} + \frac{Y_\mathrm{H} - Y_\mathrm{H,ox}}{2W_\mathrm{H}} - \frac{Y_\mathrm{O} - Y_\mathrm{O,ox}}{W_\mathrm{O}}}{\frac{2(Y_\mathrm{C,fuel} - Y_\mathrm{C,ox})}{W_\mathrm{C}} + \frac{Y_\mathrm{H,fuel} - Y_\mathrm{H,ox}}{2W_\mathrm{H}} - \frac{Y_\mathrm{O,fuel} - Y_\mathrm{O,ox}}{W_\mathrm{O}}} \quad .$$

The subscripts C, H and O correspond to the elements, the symbol W refers to their atomic masses and Y to their elemental mass fractions.

The method of chemical explosive mode analysis is described in detail by Lu et al. [8] and Shan et al. [9] . Starting from the balance equations of a chemically reacting system

$$\frac{\mathrm{D}\phi_j}{\mathrm{D}t} = \dot{\omega}_j(\phi) + S_j(\phi) \,,$$

with the material derivative $\mathrm{D}/\mathrm{D}t$, the thermodynamic variables ϕ_j, the chemical source term $\dot{\omega}_j$, and the mixing term S_j, the corresponding Jacobian $\mathbf{J}$ can be split into two parts $\mathbf{J} = \mathbf{J}_{\dot{\omega}} + \mathbf{J}_S$, where $\mathbf{J}_S$ contains the mixing contributions. The chemical Jacobian $\mathbf{J}_{\dot{\omega}}$, which is used for the following analysis, is defined as

$$\mathrm{J}_{\dot{\omega}}^{ij} = \partial\dot{\omega}_i/\partial\phi_j \,.$$

The chemistry-related information, contained in $\mathbf{J}_{\dot{\omega}}$, can be used to detect reaction zones associated with spatial or temporal changes in the explosive modes of a mixture. The eigenvalues $\boldsymbol{\lambda}$ of $\mathbf{J}_{\dot{\omega}}$ are computed as $\boldsymbol{\lambda} = \mathbf{b}\mathbf{J}_{\dot{\omega}}\mathbf{a}$, with the left and right eigenvectors $\mathbf{b}$ and $\mathbf{a}$. The eigenvalue with the largest real part is then defined as λ_e. If $\mathrm{Re}(\lambda_e)$ is positive, the eigenvalue is termed "explosive", which is a purely chemical property of the mixture. Thus, the chemical explosive mode analysis describes the reactivity of a mixture. It was demonstrated in several of the original publications [8-10] that a premixed reaction zone or homogenous ignition can be identified by a change in sign in the chemical explosive mode (CM zero-crossing), expressed as,

$$\mathrm{CM} = \mathrm{sign}\big(\mathrm{Re}(\lambda_e)\big) \times \log_{10}(1+|\,\mathrm{Re}(\lambda_e)\,|)\,,$$

where "sign" denotes the signum function.

The heat release rate (HRR) is a local quantity which can be used to detect reaction zones in laminar and turbulent flows and to determine their relative importance when multiple reaction zones occur within the same flame structure. It is calculated as

$$\mathrm{HRR} = -\,{}^{1}\!/_{\rho} \sum_{i=1}^{N_s} \dot{\omega}_i\, h_{f,i}\,,$$

with $\dot{\omega}_i$ being the chemical source term and $h_{f,i}$ being the enthalpy of formation of species i.

Note that both CM and HRR are calculated using the approximated full thermochemical state based on the Raman-accessible major species and the temperature.

3. Target flames

Two DNS databases [20, 21] of turbulent CH_4/air premixed flames are analyzed, featuring different geometrical and compositional configurations, as well as turbulence intensities, the *Bunsen flame* and the *round jet flame* configuration. Both simulations were performed using Sandia's DNS code S3D [22, 23], which solves the fully compressible Navier-Stokes, species, and energy equations with a fourth-order Runge-Kutta method for explicit time integration and an eighth-order spatial differencing scheme.

The *Bunsen flame* is a lean turbulent premixed slot flame, with an inlet temperature of T = 800 K and inlet equivalence ratio of φ = 0.7. The central slot jet is surrounded by heated co-flows on both sides, whose composition and temperature correspond to the complete adiabatic combustion products of the reactant jet. A 13-species reduced chemical mechanism [24] that is derived from the GRI-1.2 detailed mechanism is used. In addition to the 13 species that are directly computed, the concentrations of quasi-steady state species, such as CH_2, CH_2(s), HCO and CH_2OH, can be explicitly obtained through analytical expressions. The same chemical mechanism is applied in the subsequent homogeneous reactor analysis to avoid introducing errors due to differences in chemical mechanisms. A uniform grid spacing of 20 μm is employed in the streamwise and spanwise directions. The Reynolds number based on the inlet velocity and the width of the slot jet (h = 1.8 mm) is Re = 2100, and a Karlovitz number of 65 is achieved based on the Kolmogorov scale and a laminar flame scale (δ_L/s_L), which places the *Bunsen flame* in the thin reaction zone regime according to the regime diagram of turbulent premixed combustion [20]. The *Bunsen flame* is further characterized by a significant turbulence-chemistry interaction, having a turbulent Reynolds number of R_T=250 and a ratio of turbulent fluctuation to laminar burning velocity of u'/s_L =10.

The *round jet flame* is a turbulent premixed flame with a co-flowing pilot flame at atmospheric pressure. The reactant equivalence ratio is also 0.7, and the inlet jet temperature is 300 K. The co-flowing CH_4/air flame has a temperature of T = 1800 K at an equivalence ratio of φ = 0.9. With the different equivalence ratios between the reactant jet and the coflow combustion products, the *round jet flame* is a weakly stratified flame [18]. Compared to the *Bunsen flame*, the *round jet flame* is more significantly impacted by the effects of diffusive transport. A 28-species reduced chemical mechanism [8] based on GRI-Mech 3.0 is employed. Again, the same mechanism was used within the homogeneous reactor analysis. Here, a uniform grid spacing of 30 μm is used in all directions. The jet Reynolds number based on U_b and the jet diameter D (D = 1.5 mm) is 10500. Based on the same definition, the *round jet flame* has a much larger Karlovitz number (Ka = 253) than the *Bunsen flame*, and there exists a significant low-intensity heat release region downstream [4]. Thus, the *round jet flame* is placed in the broken flame regime according to the regime diagram of turbulent premixed combustion [20].

Chemical explosive mode analysis is applied to the full thermochemical states to obtain the eigenvalues of the chemical Jacobian, which serves as the benchmark data for subsequent comparison. As an example, iso-contours of instantaneous heat release rates and the chemical explosive mode are presented in Fig. 1. In both flames, the contour of significant HRR aligns closely with the CM zero-crossings (the largest eigenvalue changes sign from positive to negative). Further, the HRR reaction

regions are slightly broadened when considering the low-intensity zone, which is consistent with results shown by Wang et al. [25].

4. Comparisons of turbulent DNS with no uncertainty

For analyzing the DNS data of the turbulent flame configurations, the species measurable by Raman/Rayleigh scattering (N_2, O_2, CH_4, CO_2, H_2O, CO, H_2) and OH-LIF (OH, when included) as well as the temperature are assumed to be fixed at their initial values for each sample, and no uncertainty is imprinted based on experimentally determined uncertainties. This approach tests the accuracy of the homogeneous reactor approximation in application to high Karlovitz number turbulent flames without the added complexity of experimental uncertainty, which is analyzed in the Section 5. Results including OH as an initial condition are named "Approx. + OH"; the others are named "Approx.".

Figure 2 and Fig. 3 show the results for CM and HRR based on both approximated states ("Approx." and "Approx. + OH"), compared to results of the fully resolved DNS of the *Bunsen flame*, in the physical space and temperature space, respectively. Representative instantaneous 1D samples from the DNS (rows in Fig. 2 and Fig. 3) are chosen at various locations, including two slices along the spanwise direction $4l_t$ and $6l_t$ (center plane), where l_t is the integral length scale at the inflow conditions ($l_t = 0.45$ mm), and three heights along the streamwise direction, $4h$, $8h$ and $12h$, where h is the width of the slot jet, as defined in [4].

Each sample shows multiple CM zero-crossings as well as clearly visible local maxima in the HRR, which occur in close proximity to the CM zero-crossings. However, all four samples are characterized by a different number of CM zero-crossings and local HRR maxima. Further, there are clearly visible differences between the fully resolved DNS results and the approximated results without OH. Without using OH as a fixed input in the approximation (gray dotted line), the number of CM zero-crossings is wrongly identified for sample B#1 in Fig. 2. Further, a shift in the position of the CM zero-crossing over temperature (Fig. 3) arises in all shown samples. The HRR profiles show a good agreement of the position of the local HRR maxima. However, the maximum values tend to be over predicted by the approximation without OH, even if the magnitude is still satisfactory for some cases. This leads to a wrong characterization of the relative importance of different local reaction regimes in samples B#3 and B#4. For example, focusing on sample B#3, the second HRR peak is the most significant, based on the fully resolved results. However, the approximation without OH identifies the third local HRR peak as the most significant. When comparing in temperature space, the HRR structures are too narrow and low temperature heat release (below ~1600 K) is completely missed when not including OH in the initial state for the approximation. Despite these differences, the position of the CM zero-crossings, the values within the negative CM range as well as the position of the local HRR maxima do fit reasonably well.

When including OH in the approximation (orange dashed line), the CM and the HRR profiles give a very good qualitative and quantitative agreement with the fully resolved results. All CM zero-crossings as well as the relative importance of the local HRR maxima match, both in physical and temperature space. To support this statement, the temperature (fixed) and the heat release rate were evaluated at the positions of the CM zero-crossings in 225 independent samples for the *Bunsen flame* DNS, and the mean relative error of both approximated states to the fully resolved results was calculated. Note that even if temperature is fixed during the approximation, a shift in the CM zero-crossing translates to an offset in the corresponding temperature at the CM zero-crossing. Thus, due to the high spatial gradients of T at the CM zero-crossings, the CM shift is very prominent in T space. The mean relative error in temperature at the CM zero-crossing was 2.31 % for the approximation without OH and only 0.15 % for the approximation with OH. For the heat release rate at the CM zero-crossing, the mean relative errors were 70.83 % and 14.24 % for "Approx." and "Approx. + OH", respectively. The resulting HRRs, based on both approximations, agree with the fully resolved results within 1% when integrating across all spatial profiles. However, the approximation with OH yields much better agreement on the shape of the HRR, and for the approximation without OH offsetting errors in the profile shapes occur.

It is worth mentioning that the error arising within the temperature is clearly visibly in Fig. 3, when comparing the samples in temperature space. Based on this comparison we can conclude that when taking OH in the initial state of the approximation into account, there is a significant improvement.

Figure 4 and Fig. 5 show the results for CM and HRR, respectively, for both approximated states compared to the fully resolved DNS of the *round jet flame* configuration. Representative samples are chosen based on different axial positions of the flame (8D, 16D and 24D). As discussed in Section 3, the *round jet flame* DNS is characterized by a stratified premixed flame structure. Thus, all samples are compared in physical (distance), temperature, and mixture fraction space. Note that each sampled line originates from the axis of the burner and extends along the radial direction for the *round jet burner*. In contrast, the full transverse direction was sampled for the *Bunsen burner*.

For the three samples presented, the differences in CM, between both approximated and the fully resolved results, are slightly higher than for the *Bunsen flame*. However, this discrepancy is still relatively small and does not influence the identification of the CM zero-crossing. By considering that the negative CM values indicate the slowest-decaying modes that determine how fast the mixture relaxes to the corresponding equilibrium states, this difference might be attributable to a greater influence of diffusive transport in the stratified flame structures of the *round jet flame*.

Focusing on CM (Fig. 4), both homogeneous reactor approximations, without (gray dotted line) and with OH (orange dashed line), can correctly identify the positions of the CM zero-crossing in physical space. However, a shift in the position of the CM zero-crossing arises over temperature and mixture fraction. This shift is small when OH is included but is significant for all

samples when not including OH. For HRR (Fig. 5), the agreement of the position of the local HRR maxima is satisfying in the approximation without OH, but the maximum values are over predicted. When comparing HRR in temperature and mixture fraction space, the structure between the fully resolved and the approximated results without OH is significantly different. When including OH in the approximation (orange dashed line), the HRR profiles give a good qualitative and quantitative agreement to the fully resolved results in physical, temperature, and mixture fraction space.

Here, the temperature and the heat release rates are evaluated at the CM zero-crossing positions of 60 independent samples, and the error of the mixture fraction at the position of the CM zero-crossing is considered. The mean relative errors are found to be: 1.14 % ("Approx.") and 0.06 % ("Approx. + OH") for the temperature; 62.59 % ("Approx.") and 12.91 % ("Approx. + OH") for the heat release rate; and 0.65 % ("Approx.") and 0.18 % ("Approx. + OH") for the mixture fraction. As already discussed for the *Bunsen flame* case, the error arising for the temperature and mixture fraction is visible in Fig. 4 (middle and right), when comparing the samples in temperature and mixture fraction space. Thus, the agreement, when taking OH into account, is significantly improved. Comparing the global behavior of the HRR, the mean relative error of the integrated HRR decreases from 10.89 % for the approximation without OH to 0.51 % for the approximation with OH. Again, offsetting errors allow the integrated HRR for the approximation without OH to appear better than it should.

In summary, by using the homogeneous reactor approximation without OH, both the CM and the HRR can be assessed in a good *qualitative* manner. The spatial positions of the CM zero-crossings and the local HRR maxima were in a good agreement for all cases where the same amount of CM zero-crossings was detected. However, taking the knowledge of OH into account makes a significant difference, and we get a very good *quantitative* agreement for both HRR and CM. The accuracy of each local HRR maximum improves significantly, allowing correct assessment of the relative strength of each local HRR peak.

The correlation [OH]x[CH_2O], based on simultaneous PLIF imaging of OH and CH_2O, is widely used in turbulent flame experiments as a qualitative heat release marker to gain insight on the spatial structure of reaction zones. Similarly, [H]x[CH_2O] has been proposed as a heat release marker [4]. Therefore, it is of interest to compare the full and the approximated results for these two correlations along with HRR itself. This is done in Fig. 6 (*Bunsen flame*) and Fig. 7 (*round jet flame*), where all profiles are normalized by the maximum of the corresponding fully resolved DNS result.

The approximated results including OH (orange dashed line) agree very well with the fully resolved results for the *Bunsen flame* data and show a good quantitative agreement for the *round jet flame* DNS. Further, the values of the local maxima are well matched. In contrast, the approximation results without OH (gray dotted line) tend to over predict the peak HRR results for both cases. Thus, it is not possible to reach the right quantitative OH level at the location of peak HRR based on the approximation using only Raman accessible species.

Overall, the HRR based on the approximated results with OH yield a very good agreement with the two heat release rate indicators [OH]x[CH_2O] and [H]x[CH_2O] (all being normalized). This agrees with previous studies shown in literature. Further, when using the homogeneous reactor approximation, a very good agreement between the approximation with OH and the full results occurs for all three quantities ([OH]x[CH_2O], [H]x[CH_2O], HRR). Whereas the PLIF imaging techniques for HRR are not currently quantitative, the method proposed here has the potential to yield quantitative HRR by using Raman/Rayleigh and quantitative OH-LIF measurements, including shot-to-shot corrections for changes in local Boltzmann fraction and collisional quenching rate, combined with the homogeneous reactor approximation.

5. Effects of Experimental Uncertainty and Uncertainty Quantification

Representative experimental uncertainties in Raman/Rayleigh/CO-LIF measurements have been documented in [26] and are given in Table 1 in terms of both precision and accuracy. The methods of calibration and data processing of the experimental diagnostic system has been described recently in detail [27]. The uncertainty at each data point in the present analysis is calculated as the relative error in each species, based on the listed accuracy. Further, since these relative errors would tend to zero for near-zero mass fractions, lower bounds on uncertainty are applied, based on experimentally evaluated noise.

To identify influential uncertainties of species input to the homogeneous reactor calculation on the quantities of interest (QoI), uncertainty quantification (UQ) techniques can be applied to reduce stochastic dimension and discover model representations. In particular polynomial chaos (PC) UQ methods, developed both in the global context, employing spectral expansions spanning all of the stochastic space, and in a local context, using localized spectral representations [28], can be used. The UQ Toolkit (UQTk) [29, 30], including a collection of libraries and tools for the quantification of uncertainty in numerical model predictions, was used for the analysis shown here, allowing the variance of a QoI to be decomposed into contributions from the uncertainty of each input. Letting λ denote the vector of all input parameters, the total effect sensitivity (totsens) was computed to rank the components in terms of their variance contributions to the overall QoI $f(\lambda)$:

$$S_i = \frac{\mathbb{E}_{\lambda_i}[\mathrm{Var}_{\lambda_i}(f(\lambda)|\lambda_i)]}{\mathrm{Var}(f(\lambda))}.$$

The total effect sensitivity S_i measures the variance contributions from all terms that involve the i-th parameter and is particularly useful for determining which parameters have the most (or least) overall impact on the QoI. Unimportant parameters can be fixed at their initial values without significantly affecting the output, and the stochastic dimension can be reduced. Traditionally, these indices can be estimated via Monte Carlo approaches. As a more efficient alternative to presume a certain degree of uncertainty in the single species, polynomial chaos expansions (PCEs) were used to approximate the quantities of

interest (HRR, CM, Z). Once such PCEs are available, their orthogonal polynomial basis functions allow indices to be extracted analytically from expansion coefficients without the need of additional Monte Carlo sampling. For detailed discussions, the readers are referred to review papers and books [28, 31, 32].

Uniformly distributed uncertainty, based on the experimental accuracy and precisions of each of the seven species, was imprinted onto the whole set of input parameters (8192 realizations of the initial sample line). Then, based on the PCE UQ approach, the total effect sensitivity S_i was calculated for the mixture fraction (Z totsens), heat release rate (HRR totsens), and chemical explosive mode (CM totsens). Using this approach, the species having the greatest overall impact on the quantities of interest were identified, and a single uncertainty analysis was conducted for the input parameters.

Sample B#1, from the *Bunsen flame*, and sample R#2, from the *round jet flame*, were selected for a more detailed analysis. In Section 4, B#1 showed extra CM zero-crossings when OH was not included, and sample R#2 showed a CM zero-crossing at a relatively low temperature of roughly 1400 K. Therefore, both were expected to be sensitive to input uncertainty. Scalar profiles from these two samples are shown in Fig. 8. Sample B#1 shows more local peaks in the main species, OH, and temperature. OH, and O_2 also have much higher overall values in sample B#1. Further, the temperature range is higher in sample B#1 compared to sample R#2, where the temperature maximum is 1800 K. For a radial distance greater than 0.004 m, T, O_2 and CH_4 are constant for sample R#2, corresponding to the equilibrium products in the pilot coflow surrounding the jet.

Figures 9 and 10 show the results for Z, HRR and CM, based on the disturbed initial conditions (top row), as well as the resulting total effect sensitivity (bottom row) for the *Bunsen flame* sample B#1 and the *round jet flame* sample R#2, respectively. The black line in the top row indicates the undisturbed reference, while the gray areas shows the range of results based on the disturbed inputs. Starting with the mixture fraction in Fig. 9, a nearly constant offset of about +/- 4 % arises. The mixture fraction has a straightforward dependence on species uncertainties as dictated by its linear formulation. Note, that the *Bunsen flame* configuration is non-stratified, however, variations in mixture fraction arise due to combined effects of differential diffusion and calculation of Z from major species only. Within the spatial range of -0.001 m to 0.0 m, where relatively low temperature occurs, O_2 and CH_4 are the main contributors to mixture fraction uncertainty (row 2 in Fig. 9). Within the reaction zones, CO becomes an important contributor to Z uncertainty, due to its high local concentrations and relatively large experimental uncertainty (accuracy) of 10%. In contrast to the mixture fraction, HRR and CM are, depending on the initial state, highly sensitive to the input uncertainty. Significant differences occur for the HRR, especially in regions outside the reaction zones, where the reference value is zero or near-zero. For regions corresponding to the reactant jet, OH is the primary contributor to HRR uncertainty, since OH values should be zero or near-zero. Thus, imposed uncertainty produces a large relative change in OH, which strongly influences the HRR. In the outer regions corresponding to the pilot products, CH_4 is the primary contributor to HRR uncertainty. Again, since CH_4 should be zero or near-zero, the imposed uncertainty causes large relative changes. Moreover, CM is relatively insensitive to input uncertainty across most of the B#1 profile, except in the region of reactants, where the reference values are zero or slightly positive, and near -0.002 m, where there are local peaks in T and OH. Within the reactant region, OH is the main contributor to uncertainty, with unphysical positive OH values causing CM to become negative. Further, the location near -0.002 m is close to a tipping point in the chemical explosive mode, and there are several species that contribute to the CM uncertainty. For instance H_2 is shown to be an important contributor to CM uncertainty, exceeding the influence of OH in some locations. However, the relative effect of H_2 is only high in regions where the resultant uncertainty in CM is quite small.

Figure 10 shows the results of the disturbed QoIs and the total sensitivity for the *round jet flame* sample R#2. The offset in mixture fraction is nearly constant at about +/- 2%. The main contributor to uncertainty in the mixture fraction is O_2, followed by CH_4, H_2 and CO, with the latter two contributing due to there relatively large experimental uncertainties (both at 10%). As for the *Bunsen flame* sample, the HRR shows significant sensitivity to CH_4 and to OH uncertainty, where the reference CH_4 or reference OH value is zero, respectively. In contrast to the *Bunsen* flame sample, sample R#2 has a large region where the reference CM is zero (distance > 0.004 m). Within this region, large errors in the disturbed CM profiles come mainly from H_2 uncertainty where the reference H_2 is near-zero, and the worst case imprinted error in H_2 is 1e-4, compared to the maximum value in sample R#2 of roughly 4e-4. Compared to sample B#1, sample R#2 shows a higher CM sensitivity to CH_4 within the negative CM regions, and the sensitivity to OH is correspondingly reduced. However, the locations of the three CM zero-crossings in the reference profile and the areas of positive CM are relatively insensitive to the imposed input uncertainties.

In both samples, CH_4, H_2 and OH are the species having greatest influence on CM and HRR results derived from the approximated full thermochemical state from the homogeneous reactor calculation. In the following, these three species are disturbed separately by a fixed positive and negative offset calculated for each 1D sample as relative percentage of the local mass fraction, based on uncertainty from Table 1 and taking the lower bound on precision into account. This approximates the combination of mean uncertainty in calibrated system response (accuracy) and measurement noise (precision).

Figure 11 shows profiles of Z, HRR, and CM for the reference, added positively uncertainty, and added negative uncertainty for each of the three species, CH_4, H_2 and OH. First, CH_4 and H_2 do influence the mixture fraction for both samples. Since Z is based on the overall C, H and O balance, this was to be expected. Further, these profiles specifically help to clarify physical reasons behind the sensitivities observed above for HRR and CM. It becomes apparent that a positive offset in CH_4 causes HRR to increase in regions where the reference mass fraction of CH_4 is zero or near-zero, as in sample B#1 at each end of the profile. Conversely, an imposed decrease in CH_4 reduces HRR, unless CH_4 or HRR is already zero. The HRR is insensitive to uncertainty in CH_4 when the CH_4 mass fraction is much larger that the imposed uncertainty, as for the range between 0.002 m and 0.0035 m in sample R#2. In a similar way, HRR is sensitive to OH uncertainty when the reference OH mass fraction is zero or near-zero. For example, HRR increases near the middle of each of the two sample profiles when a positive offset in OH is imposed.

CM is relatively insensitive to CH_4 and H_2, except in the region on the right end of the sample R#2, where the reference values for CM and HRR are both zero. Here, both CH_4 and H_2 are zero or near-zero, so the imposed positive offset causes a large relative change in the mass fraction (while negative offsets make no difference). Thus, results for both HRR and CM are relatively insensitive to H_2 in the active parts of both flames. In sample B#1, a positive offset in OH produces extra CM zero-crossings. As discussed above, the extra CM zero-crossings near -0.002 m align with local maxima in OH and *T*, and the extra OH is sufficient to change the chemical explosive mode from explosive to non-explosive. For the extra CM zero-crossings near -0.0015 m and 0.0 m, the local conditions are also in a sensitive range for the chemical explosive mode.

Overall, the greatest sensitivities in HRR and CM occur in regions where either OH or CH_4 has mass fractions zero or near-zero. This points to the need to achieve best possible single-shot accuracy in measurements of CH_4 and OH at low levels. However, this sensitivity analysis also raises the possibility of identifying non-physical values of these key species, particularly finite values of CH_4 or OH due to noise, when measurements of temperature and the other species indicate that zero or negligibly small values of CH_4 or OH should be expected.

Further, the prediction of a quantitative HRR by including OH for future measurements in highly turbulent flames is still very promising, however, care has to be taken to limit the experimental uncertainty of the most influential species.

6. Summary and Conclusion

Direct numerical simulation (DNS) data from two high-Karlovitz-number methane-air flames, a premixed Bunsen flame and a stratified-premixed round jet flame, have been used to evaluate the potential applicability of a recently-developed method for approximating the local chemical explosive mode (CM) and heat release rate (HRR) starting from experimentally determined temperature and major species (CH_4, O_2, N_2, CO_2, H_2O, CO, H_2). For each DNS sample, these scalars were extracted and used as initial state for a constrained homogeneous reactor calculation, which produced a pointwise approximation of the original full thermochemical state. The CM and HRR calculated from this approximated state were compared to those calculated from the fully resolved DNS. Additionally, the impact of including the experimentally accessible OH radical as an input to the homogeneous reactor approximation was considered to improve the estimation of the CM and HRR.

Results showed that the CM and the HRR can be recovered in a good qualitative manner without including OH as an input to the approximation procedure. Specifically, spatial locations of CM zero-crossings and HRR peak locations were reasonably well captured, while HRR values at those peaks were over predicted by the approximation without OH. When OH was included as an input to the approximation, the accuracy of the recovered HRR improved significantly, giving close quantitative agreement with the DNS for both the Bunsen burner and the round jet configuration. The accuracy in the CM profiles and the positions of the CM zero-crossings was also improved, giving close quantitative agreement with the DNS. Thus, adding information of quantitative OH led to a highly accurate representation of the heat release rate and the chemical explosive mode when no uncertainty in the inputs is considered. This further validates the constrained homogeneous reactor approximation as a method for determining CM and HRR from experimental data.

When including the effect of experimental uncertainty, it was shown that changes in the initial conditions can significantly influence the magnitude of the HRR and the number of CM zero-crossings. Results are especially sensitive when unphysical effects arise from experimental uncertainty, such as finite values for sensitive species that should not be present. Strategies will need to be developed allowing the species to relax within the bounds of reported experimental uncertainties and criteria have to be worked out based on the accuracy arising in the specific sample lines.

Overall, the CM results for CM zero-crossing locations as well as the whole CM range are represented well by the approximation and are relatively insensitive to uncertainty in the input species.

Broadly, the present work establishes the potential to derive quantitative information on the chemical explosive mode and the heat release rate from 1D Raman/Rayleigh/OH-LIF experiments in turbulent flames having strong effects of turbulence chemistry interaction (high Karlovitz number). This represents a significant advance.

7. Acknowledgments

The authors acknowledge informative and insightful discussions about UQ and the help with UQTk with H. N. Najm and X. Huan. Further, the authors acknowledge assistance by Peiyu Zhang for data generation and visualization. The authors acknowledge funding by the Deutsche Forschungsgemeinschaft (DFG, German Research Foundation) - Projektnummer 325144795. S. Hartl gratefully acknowledges funding received through the equality concept scholarship of the University of Applied Science Darmstadt. R. Barlow acknowledges partial support from the U.S. Department of Energy, Office of Basic Energy Sciences, Division of Chemical Sciences, Geosciences, and Biosciences. Sandia National Laboratories is a multi-mission laboratory managed and operated by National Technology and Engineering Solutions of Sandia, LLC., a wholly owned subsidiary of Honeywell International, Inc., for the U.S. Department of Energy's National Nuclear Security Administration under contract DE-NA-0003525. Acknowledgment is also made to the Donors of the American Chemical Society Petroleum Research Fund for partial support of this research.

8. References

[1] S. Hartl, D. Geyer, A. Dreizler, G. Magnotti, R.S. Barlow, C. Hasse, Regime identification from Raman/Rayleigh line measurements in partially premixed flames, Combust. Flame 189 (2018) 126-141.

[2] S. Hartl, R. Van Winkle, D. Geyer, A. Dreizler, G. Magnotti, C. Hasse, R.S. Barlow, Assessing the relative importance of flame regimes in Raman/Rayleigh line measurements of turbulent lifted flames, Proc. Combust. Inst. 37 (2019) 2297 - 2305.
[3] K. Kohse-Höinghaus, R.S. Barlow, M. Aldén, J. Wolfrum, Combustion at the focus: laser diagnostics and control, Proc. Combust. Inst. 30 (2005) 89-123.
[4] T.M. Wabel, P. Zhang, X. Zhao, H. Wang, E.R. Hawkes, A.M. Steinberg, Assessment of chemical scalars for heat release rate measurement in highly turbulent premixed combustion including experimental factors, Combust. Flame 194 (2018) 485–506.
[5] I.A. Mulla, A. Dowlut, T. Hussain, Z.M. Nikolaou, S.R. Chakravarthy, N. Swaminathan, R. Balachandran, Heat release rate estimation in laminar premixed flames using laser-induced fluorescence of CH2O and H-atom, Combust. Flame 165 (2016) 373-383.
[6] H.N. Najm, P.H. Paul, C.J. Mueller, P.S. Wyckoff, On the Adequacy of Certain Experimental Observables as Measurements of Flame Burning Rate, Combust. Flame 113 (1998) 312-332.
[7] P.H. Paul, H.N. Najm, Planar laser-induced fluorescence imaging of flame heat release rate, Symposium (International) on Combustion 27 (1998) 43-50.
[8] T.F. Lu, C.S. Yoo, J.H. Chen, C.K. Law, Three-dimensional direct numerical simulation of a turbulent lifted hydrogen jet flame in heated coflow: a chemical explosive mode analysis, J. Fluid Mech. 652 (2010) 45-64.
[9] R. Shan, C.S. Yoo, J.H. Chen, T. Lu, Computational diagnostics for n-heptane flames with chemical explosive mode analysis, Combust. Flame 159 (2012) 3119-3127.
[10] I.A. Dodoulas, S. Navarro-Martinez, Analysis of extinction in a non-premixed turbulent flame using large eddy simulation and the chemical explosion mode analysis, Combust. Theor. Model. 19 (2015) 107-129.
[11] B. Wu, X. Zhao, C. Xu, T. Lu, Analysis of The Chemical States of A Bluff-body Stabilized Premixed Flame Near Blowoff, AIAA Scitech 2019 Forum, San Diego, California, 2019.
[12] T.M. Wabel, A.W. Skiba, J.F. Driscoll, Turbulent burning velocity measurements: Extended to extreme levels of turbulence, Proc. Combust. Inst. 36 (2017) 1801–1808.
[13] F.T.C. Yuen, Ö.L. Gülder, Turbulent premixed flame front dynamics and implications for limits of flamelet hypothesis, Proc. Combust. Inst. 34 (2013) 1393–1400.
[14] A.W. Skiba, T.M. Wabel, C.D. Carter, S.D. Hammack, J.E. Temme, J.F. Driscoll, Premixed flames subjected to extreme levels of turbulence part I: Flame structure and a new measured regime diagram, Combust. Flame 189 (2018) 407–432.
[15] B. Zhou, C. Brackmann, Q. Li, Z. Wang, P. Petersson, Z. Li, M. Aldén, B. X., Distributed reactions in highly turbulent premixed methane/air flames: Part I. Flame structure characterization. , Combust. Flame 162 (2015) 2937-2953.
[16] B.R. Chowdhury, B.M. Cetegen, Effects of fuel properties and free stream turbulence on characteristics of bluff-body stabilized flames, Combust. Flame 194 (2018) 206-222.
[17] T.M. Wabel, A.M. Steinberg, R.S. Barlow, Multi-Scalar Measurements of Premixed Flames in Extreme Turbulence Using Raman/Rayleigh Diagnostics, AIAA Scitech 2019 Forum, San Diego, California, 2019.
[18] H. Wang, E.R. Hawkes, B. Savard, J.H. Chen, Direct numerical simulation of a high Ka CH4/air stratified premixed jet flame, Combust. Flame 193 (2018) 229-245.
[19] R.W. Bilger, S.H. Sterner, R.J. Kee, On reduced mechanisms for methane air combustion in nonpremixed flames, Combust. Flame 80 (1990) 135-149.
[20] R. Sankaran, E.R. Hawkes, C.S. Yoo, J.H. Chen, Response of flame thickness and propagation speed under intense turbulence in spatially developing lean premixed methane–air jet flames, Combust. Flame 162 (2015) 3294–3306.
[21] H. Wang, E.R. Hawkes, B. Zhou, J.H. Chen, Z. Li, M. Aldén, A comparison between direct numerical simulation and experiment of the turbulent burning velocity-related statistics in a turbulent methane-air premixed jet flame at high Karlovitz number, Proc. Combust. Inst. 36 (2017) 2045-2053.
[22] J.H. Chen, Petascale direct numerical simulation of turbulent combustion—fundamental insights towards predictive models., Proc. Combust. Inst. 33 (2011) 99–123.
[23] J.H. Chen, A. Choudhary, B. de Supinski, M. DeVries, E.R. Hawkes, S. Klasky, W.K. Liao, K.L. Ma, J. Mellor-Crummey, P. N., S. R., S. S., Y.C. S, Terascale direct numerical simulations of turbulent combustion using S3D., Computational Science & Discovery 2 (2009) 015001.
[24] R. Sankaran, E.R. Hawkes, J.H. Chen, T. Lu, C.K. Law, Structure of a spatially developing turbulent lean methane–air Bunsen flame, Proc. Combust. Inst. 31 (2007) 1291–1298.
[25] H. Wang, E.R. Hawkes, J.H. Chen, A direct numerical simulation study of flame structure and stabilization of an experimental high Ka CH4/air premixed jet flame, Combust. Flame 180 (2017) 110-123.
[26] R.S. Barlow, S. Meares, G. Magnotti, H. Cutcher, A.R. Masri, Local extinction and near-field structure in piloted turbulent CH4/air jet flames with inhomogeneous inlets, Combust. Flame 162 (2015) 3516-3540.
[27] R.S. Barlow, M.J. Dunn, M.S. Sweeney, S. Hochgreb, Effects of preferential transport in turbulent bluff-body-stabilized lean premixed CH4/air flames, Combustion and Flame 159 (2012) 2563-2575.
[28] H.N. Najm, Uncertainty Quantification and Polynomial Chaos Techniques in Computational Fluid Dynamics, Annual Review of Fluid Mechanics 41 (2009) 35-52.
[29] B.J. Debusschere, H.N. Najm, P.P. Pébay, O.M. Knio, R.G. Ghanem, O.P.L. Maître, Numerical Challenges in the Use of Polynomial Chaos Representations for Stochastic Processes, SIAM J. Sci. Comput. 26 (2004) 698–719.

[30] R.G. Ghanem, D. Higdon, H. Owhadi, Handbook of Uncertainty Quantification, Springer International Publishing2017.
[31] O. Le Maitre, O.M. Knio, Spectral Methods for Uncertainty Quantification, Springer Netherlands2010.
[32] D. Xiu, Fast Numerical Methods for Stochastic Computations, Computational Physics 5 (2009) 242-272.

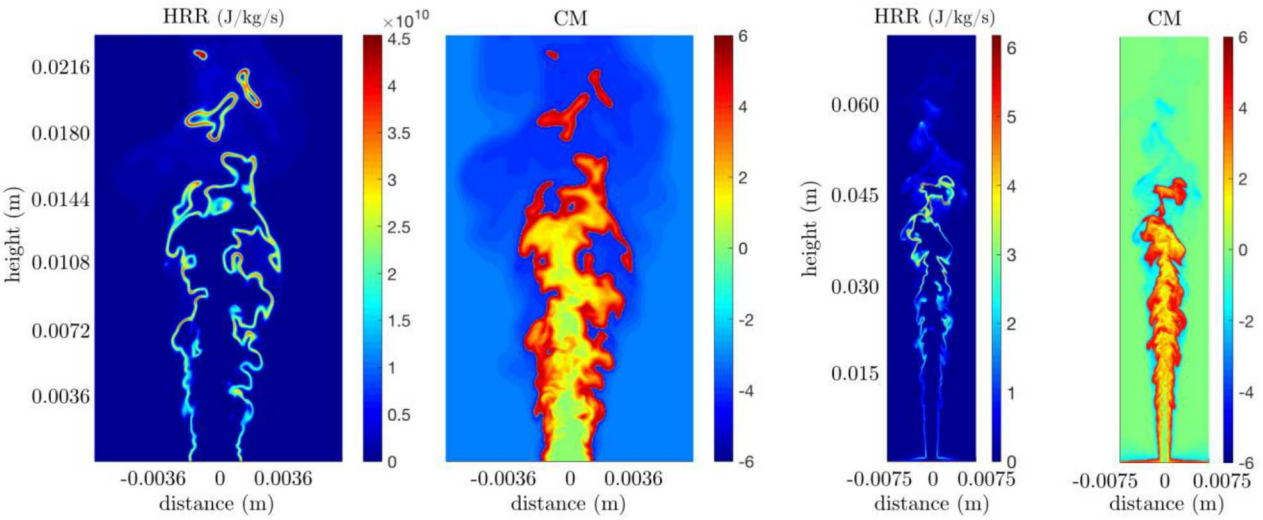

(a) *Bunsen flame*, HRR (b) *Bunsen flame*, CM (c) *round jet flame*, HRR (d) *round jet flame*, CM

Fig. 1: *Iso-contours of heat release rates and chemical explosive mode for the two test flames.*

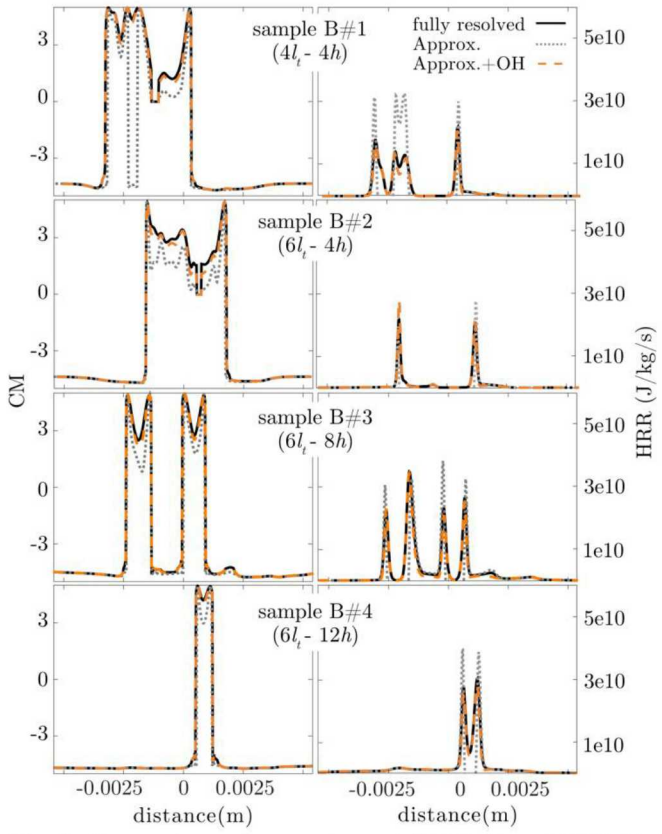

Fig. 2: *Comparison of approximated CM (left) and HRR (right) to the fully resolved solution for representative 1D samples of the Bunsen flame configuration in physical space.*

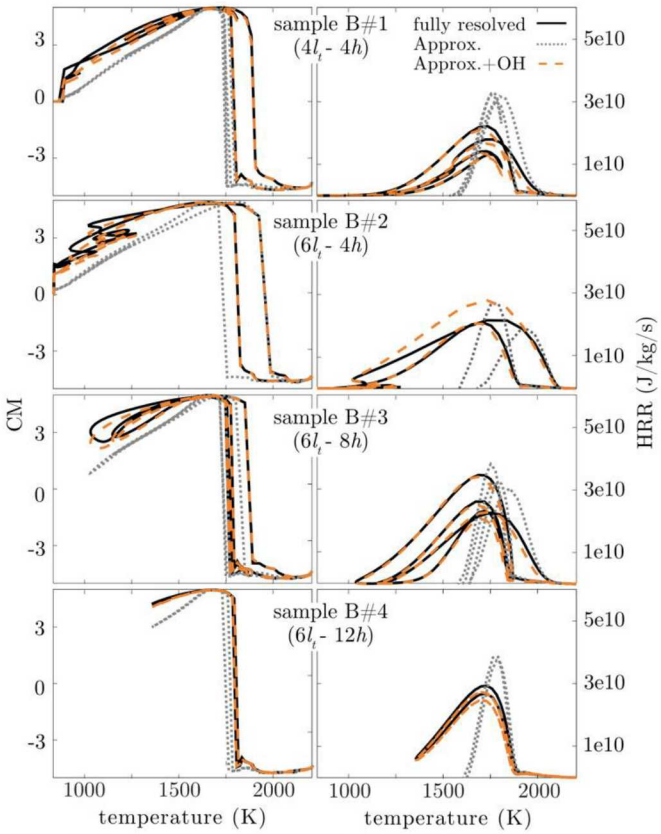

Fig. 3: *Comparison of approximated CM (left) and HRR (right) to the fully resolved solution for representative 1D samples of the Bunsen flame configuration over temperature.*

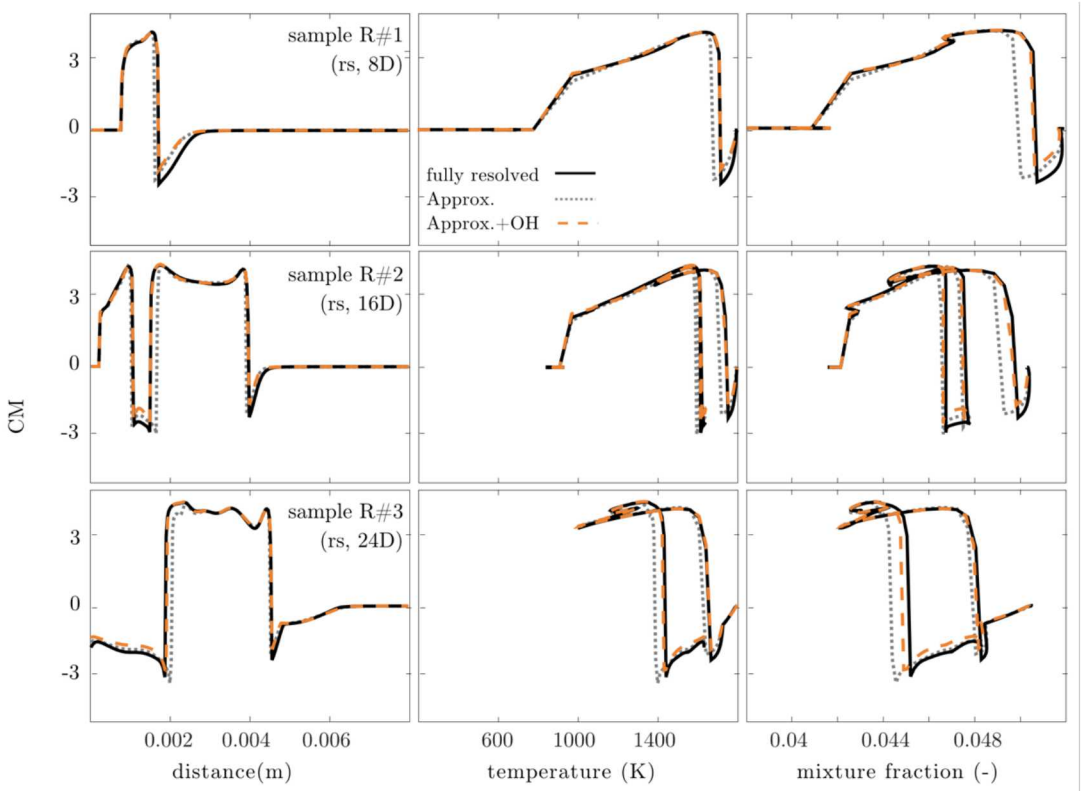

Fig. 4: *Comparison of approximated CM to the fully resolved solution for representative samples of the round jet flame configuration over distance (left), temperature (middle) and mixture fraction (right).*

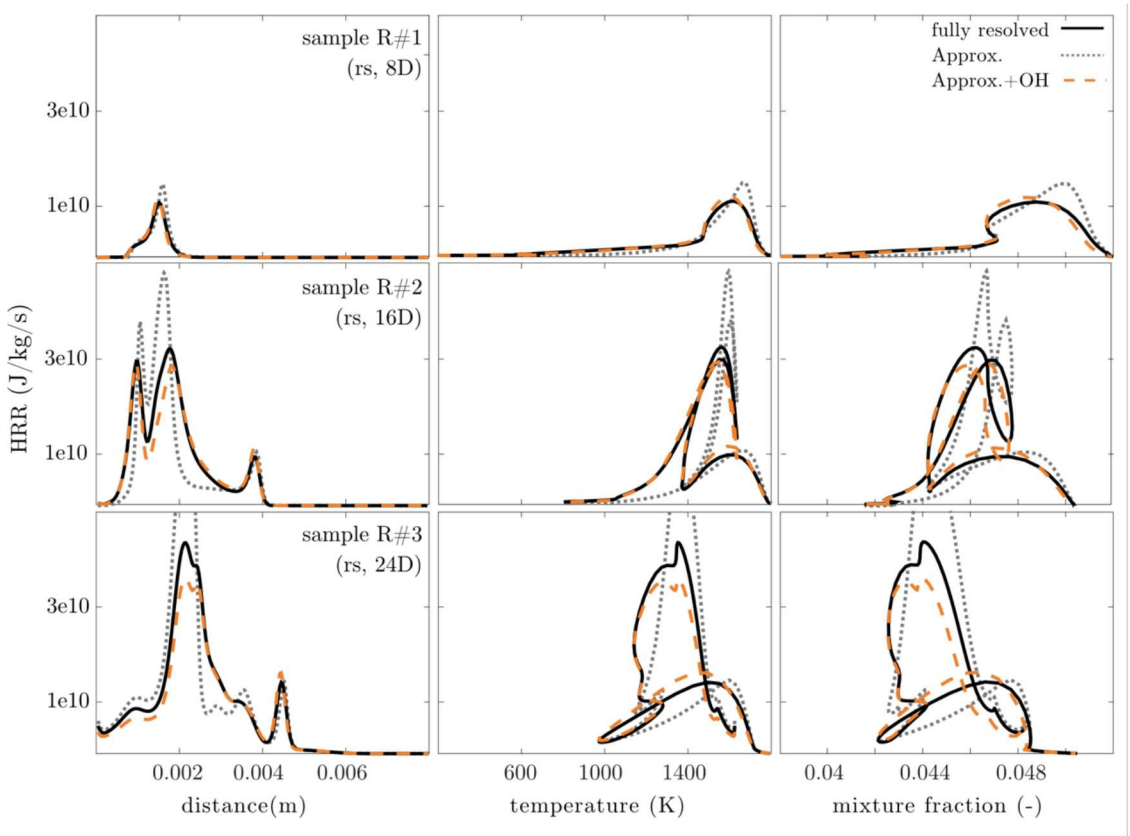

Fig. 5: *Comparison of approximated HRR to the fully resolved solution for representative sample of the round jet flame configuration over distance (left), temperature (middle) and mixture fraction (right).*

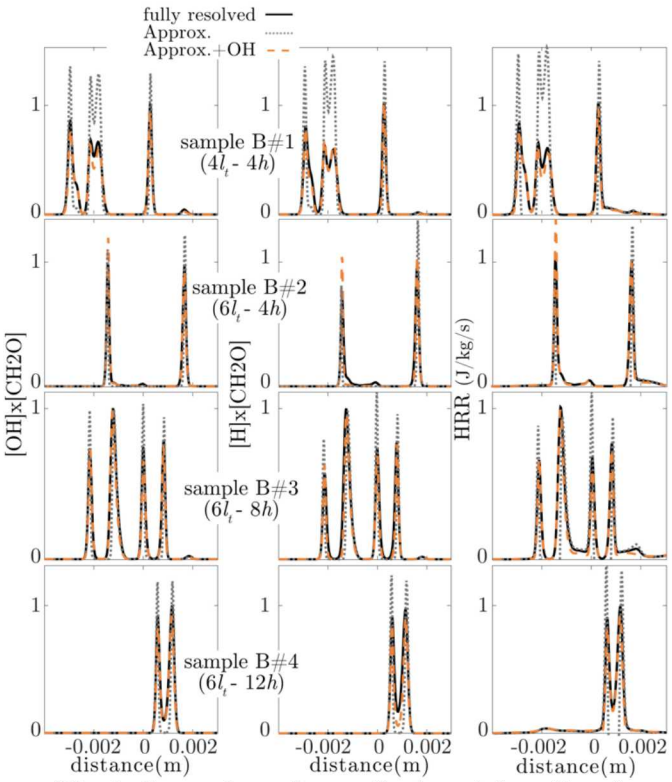

Fig. 6: *Comparison of normalized spatial profiles of [OH]x[CH₂O] (left), [H]x[CH₂O] (middle), and HRR (right) for representative samples from the Bunsen flame.*

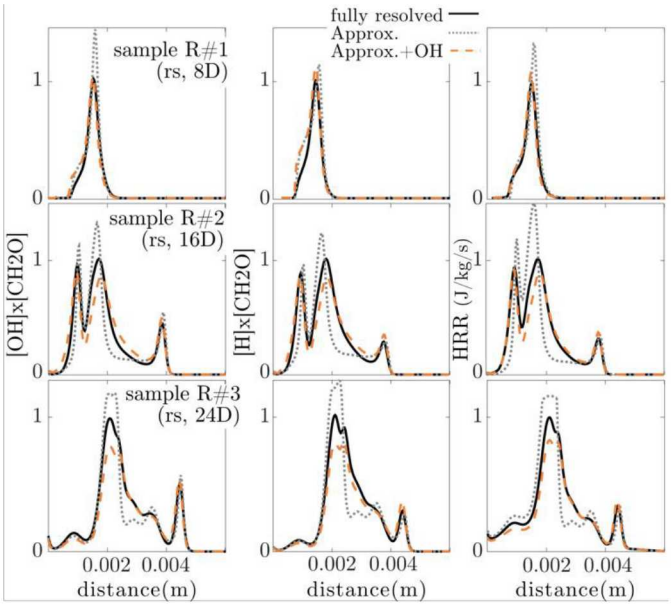

Fig. 7: *Comparison of normalized spatial profiles of [OH]x[CH2O] (left), [H]x[CH₂O] (middle), and HRR (right) for representative samples from the jet flame.*

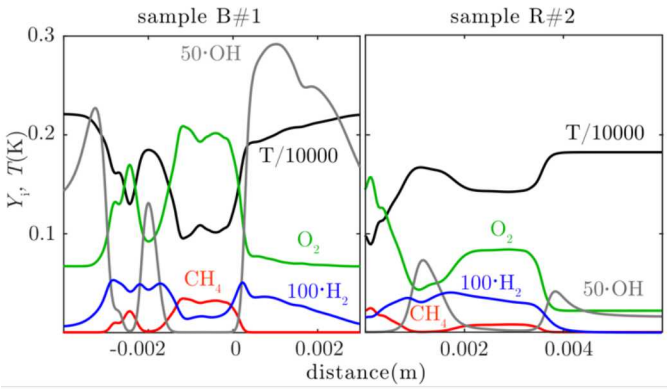

Fig. 8: *Species and temperature profiles for the Bunsen flame (sample B#1) and the round jet flame (sample R#2) configuration.*

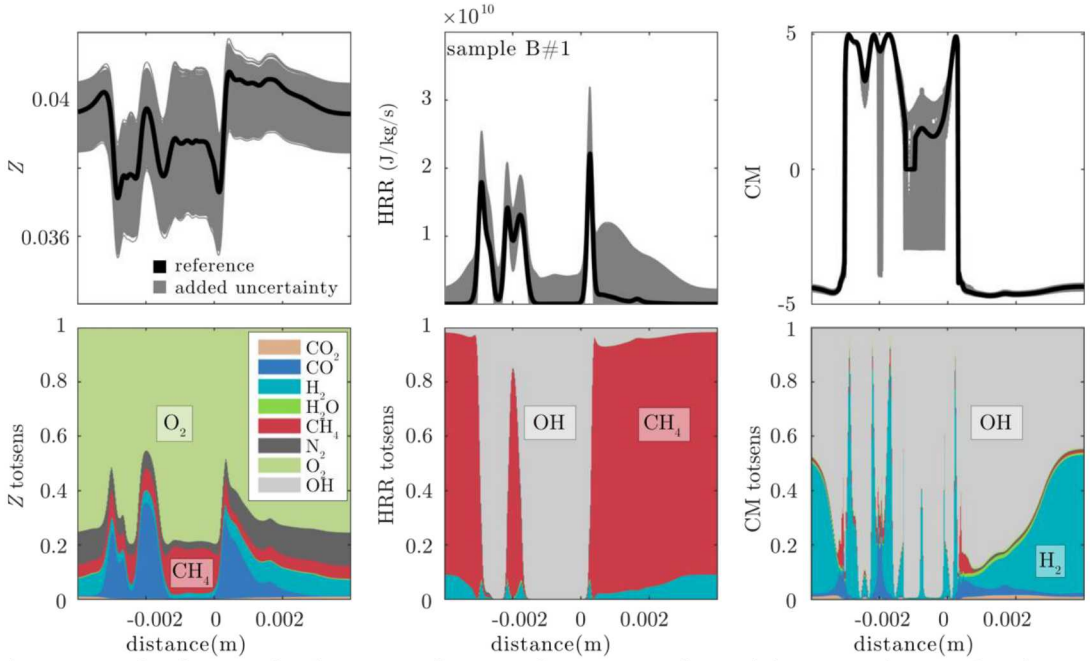

Fig. 9: *Total sensitivity for the QoIs for the Bunsen flame configuration in the model error study. Results of Z, HRR and CM, based on the disturbed initial conditions, are shown in the top row and the resulting total effect sensitivity in the bottom row.*

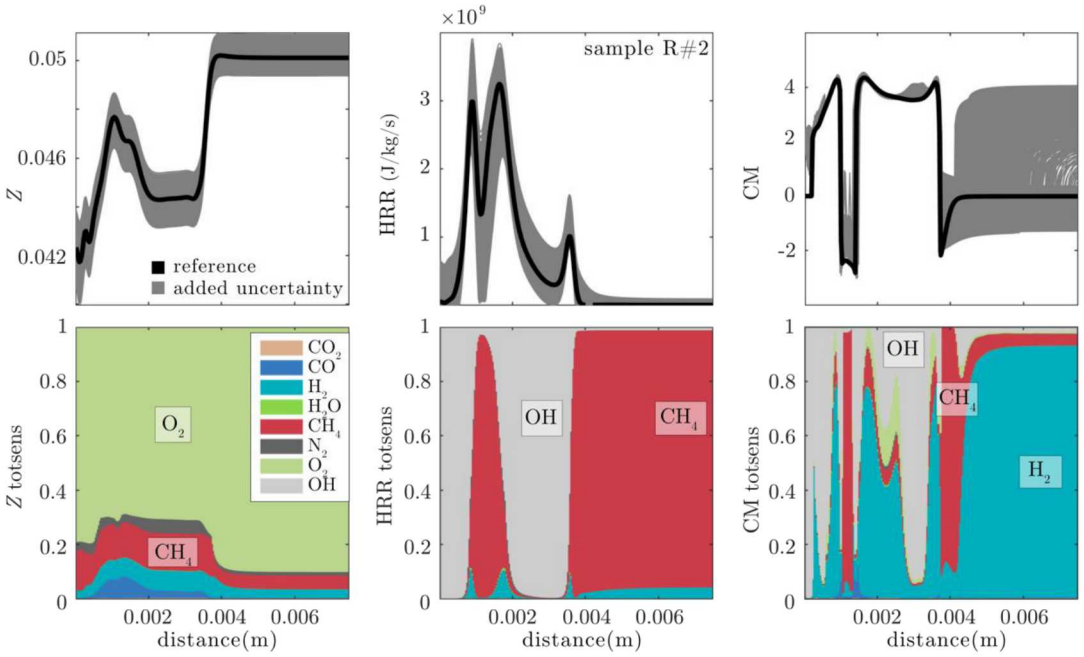

Fig. 10: *Total sensitivity for the QoIs for the round jet flame configuration in the model error study. Results of Z, HRR and CM, based on the disturbed initial conditions, are shown in the top row and the resulting total effect sensitivity in the bottom row.*

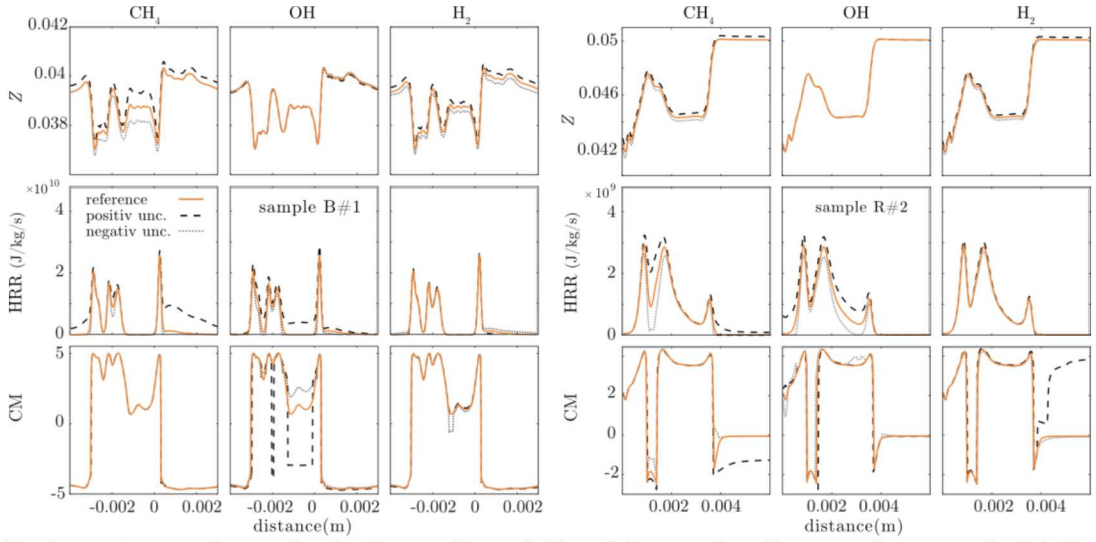

Fig. 11: *Single species pertubation for the Bunsen flame (left) and the round jet flame configuration (right). Results of Z, HRR and CM, based on the disturbed initial conditions (CH_4, OH and H_2), are shown.*

Table 1: *Representative uncertainties in scalar measurements at specific flame and cold-flow conditions.*

Scalar	Precision, σ	Accuracy	Premixed conditions
T	0.7%	2 %	$\varphi = 0.97$, $T = 2185$ K
N_2	0.6%	2 %	$\varphi = 0.97$, $T = 2185$ K
CO_2	2.5%	4 %	$\varphi = 0.97$, $T = 2185$ K
H_2O	1.7%	3 %	$\varphi = 0.97$, $T = 2185$ K
φ, Z	2.0%	5 %	$\varphi = 0.97$, $T = 2185$ K
CO	3.3%	10 %	$\varphi = 1.28$, $T = 2045$ K
H_2	5.5%	10 %	$\varphi = 1.28$, $T = 2045$ K
CH_4	0.6%	2 %	$\varphi = 1.28$, $T = 294$ K
O_2	0.7%	3 %	$\varphi = 1.28$, $T = 294$ K
OH	-	10 %	-

Figure 1

Click here to access/download;Figure;Fig1.pdf

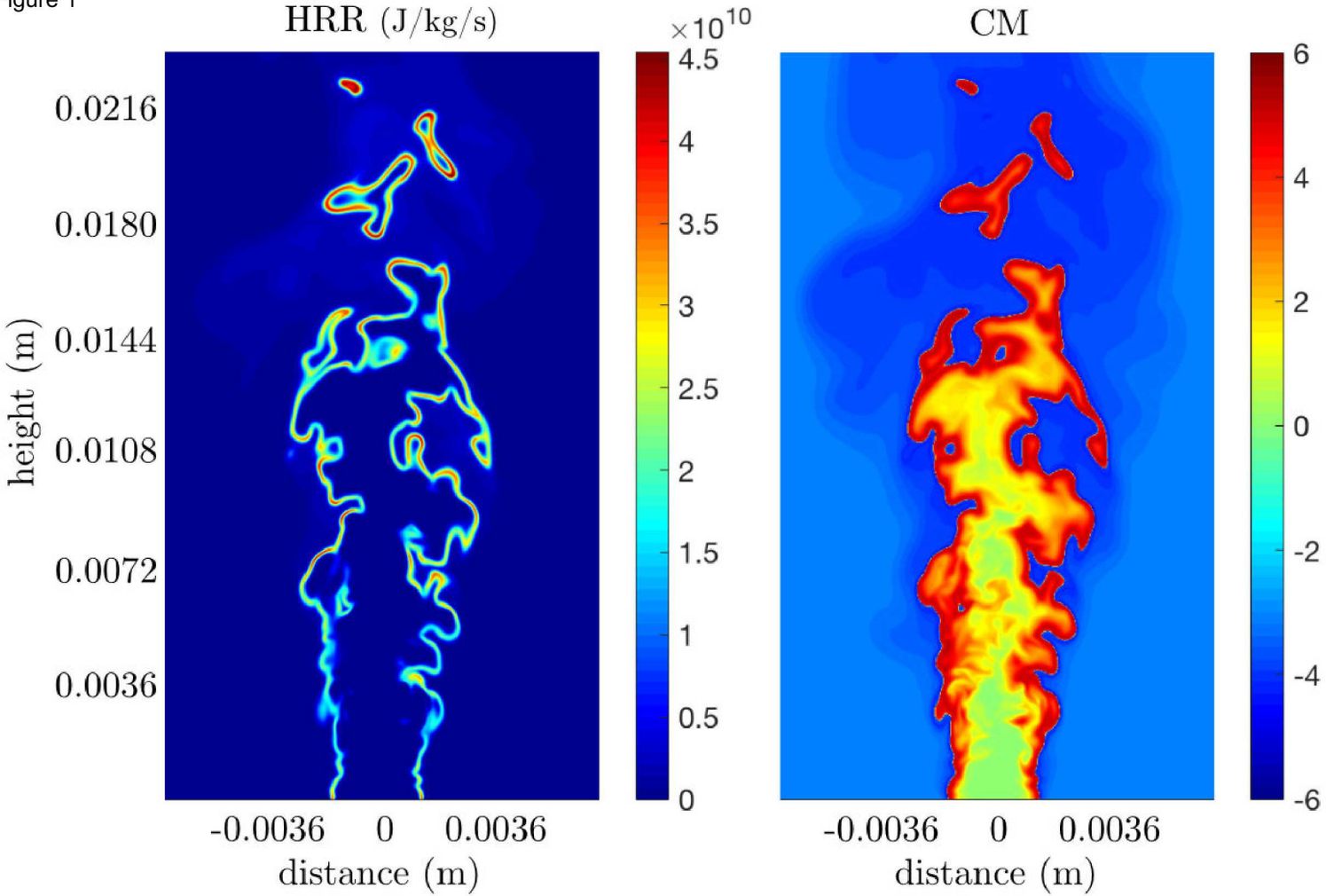

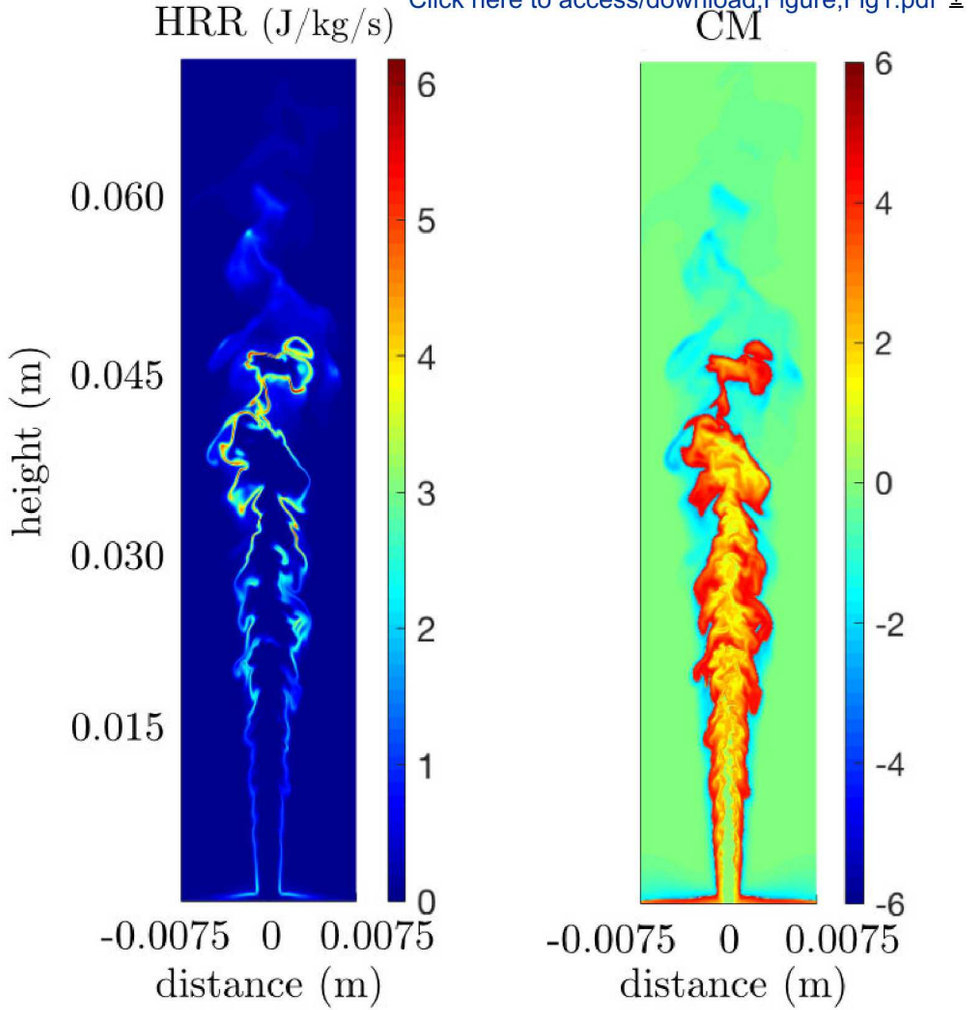

Figure 2

Click here to access/download;Figur

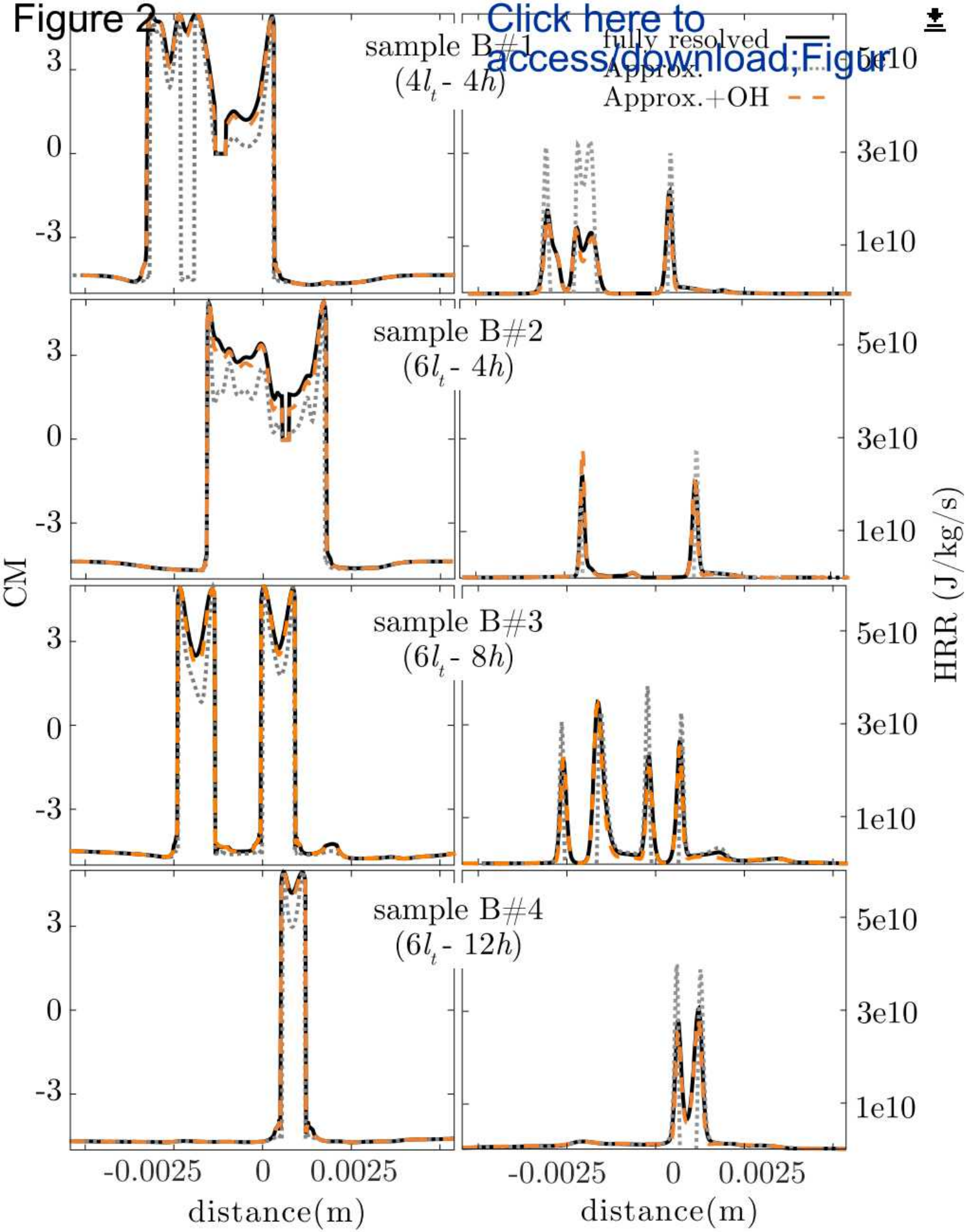

Figure 3

Click here to access/download;Figur

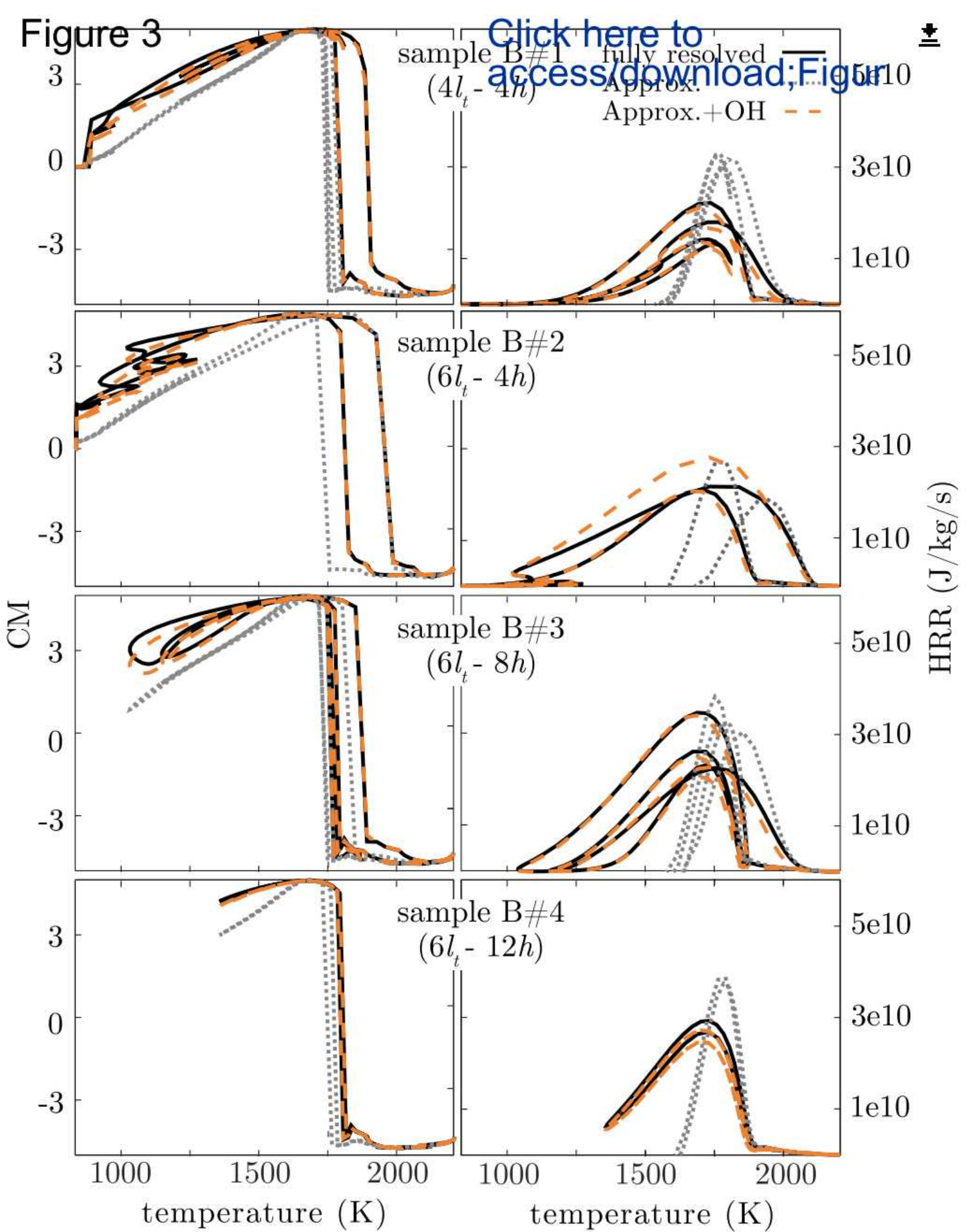

Figure 4

Click here to access/download;Figure;Fig4_HRR_Lun

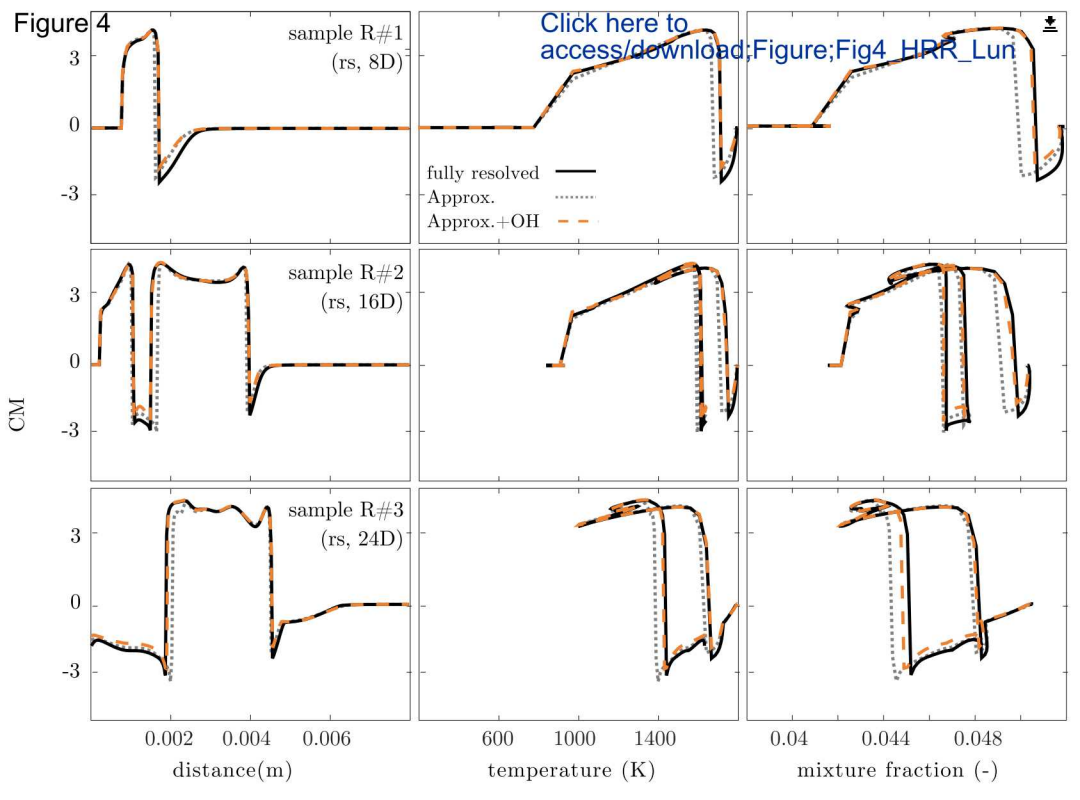

Figure 5

Click here to access/download;Figure;Fig5_HRR_Lun

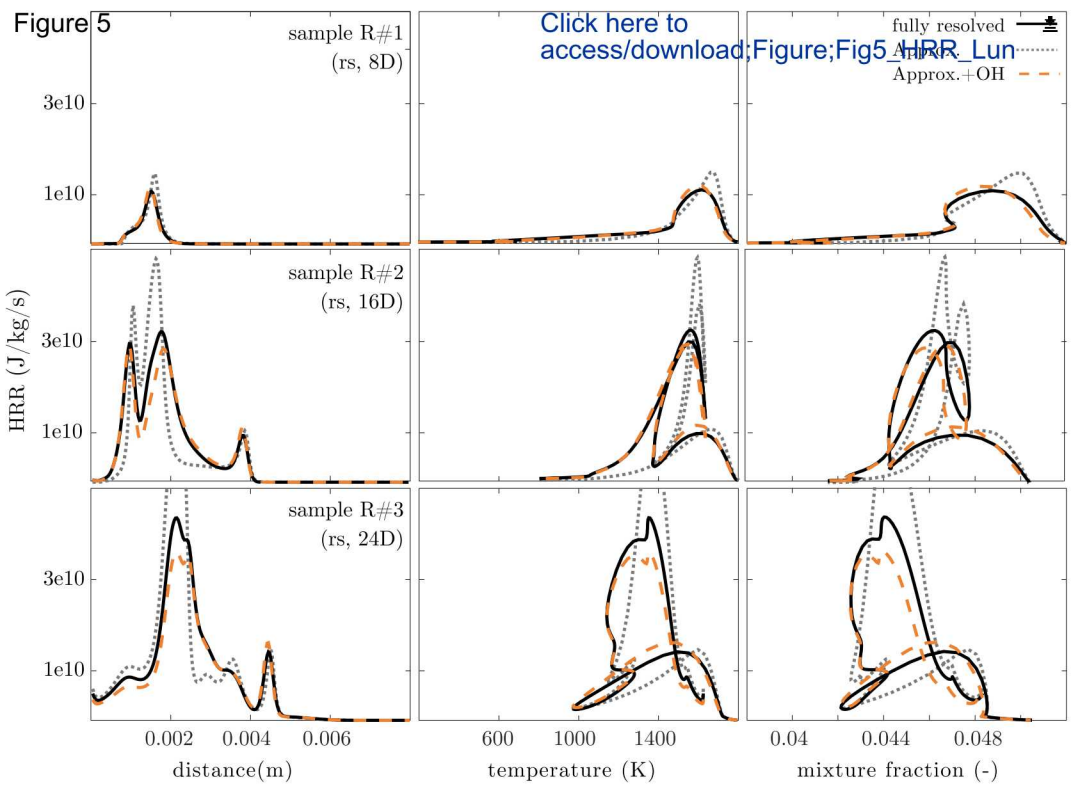

Figure 6

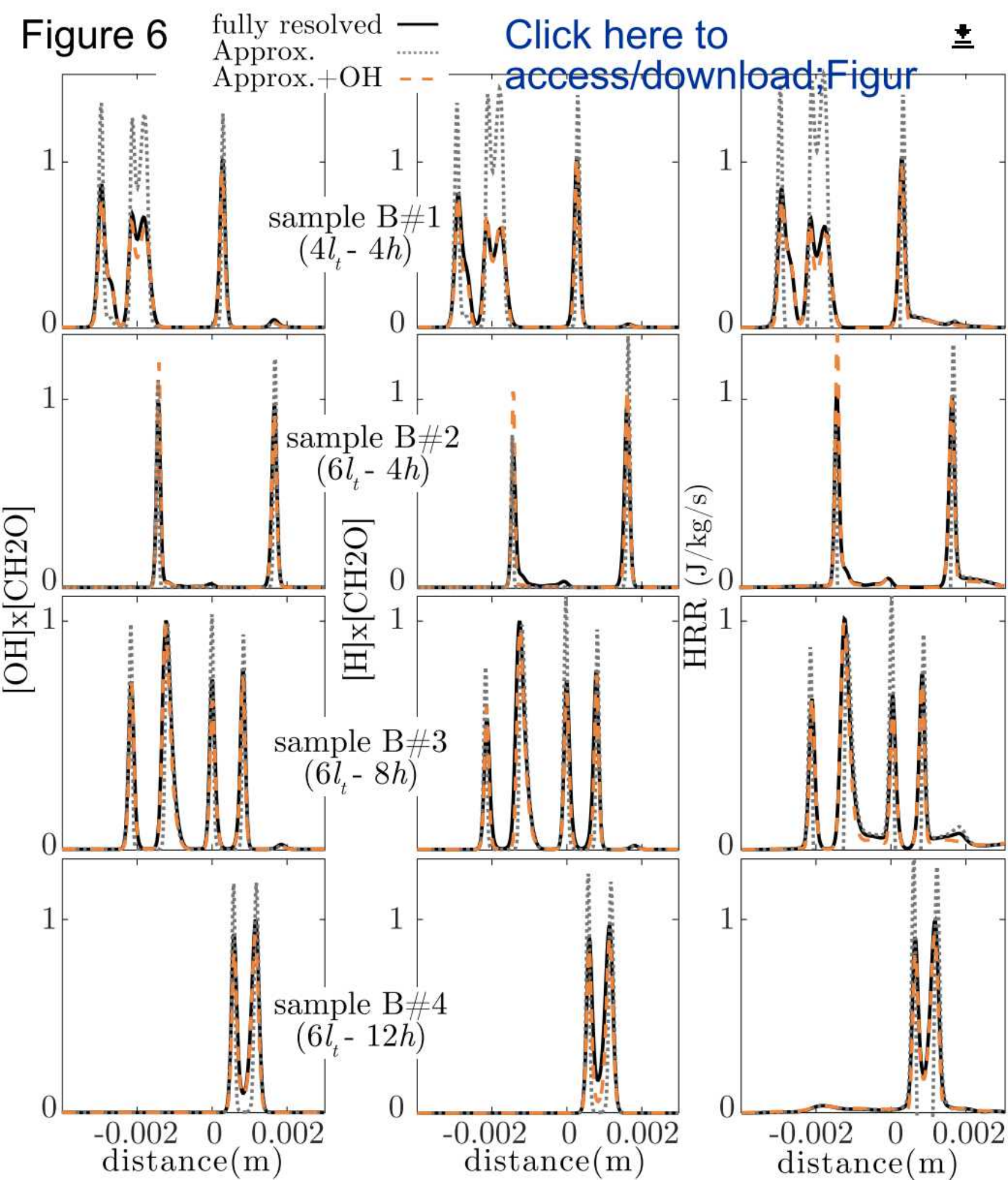

Click here to access/download;Figur

Figure 7

Click here to access/download;Figur

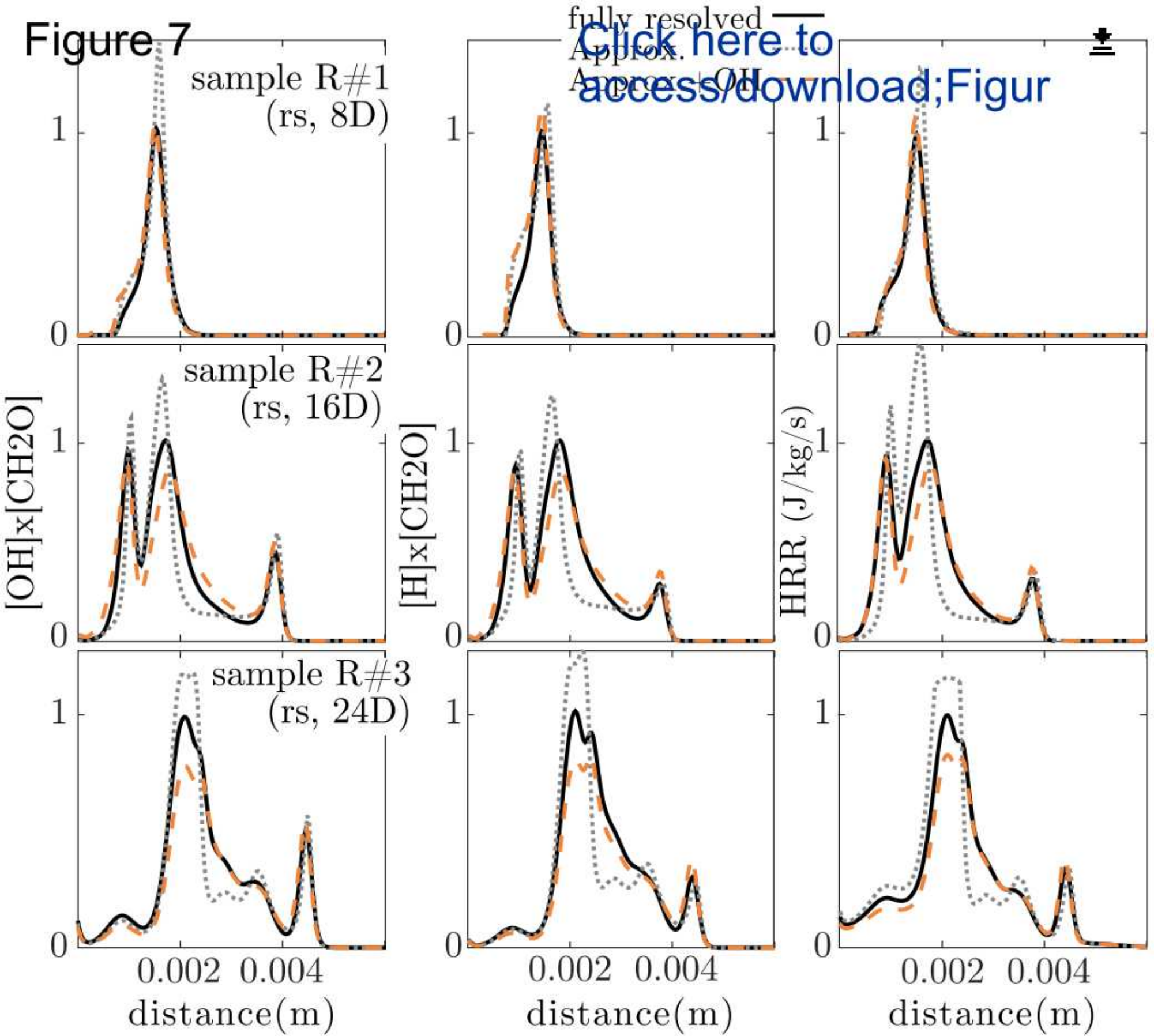

Figure 8

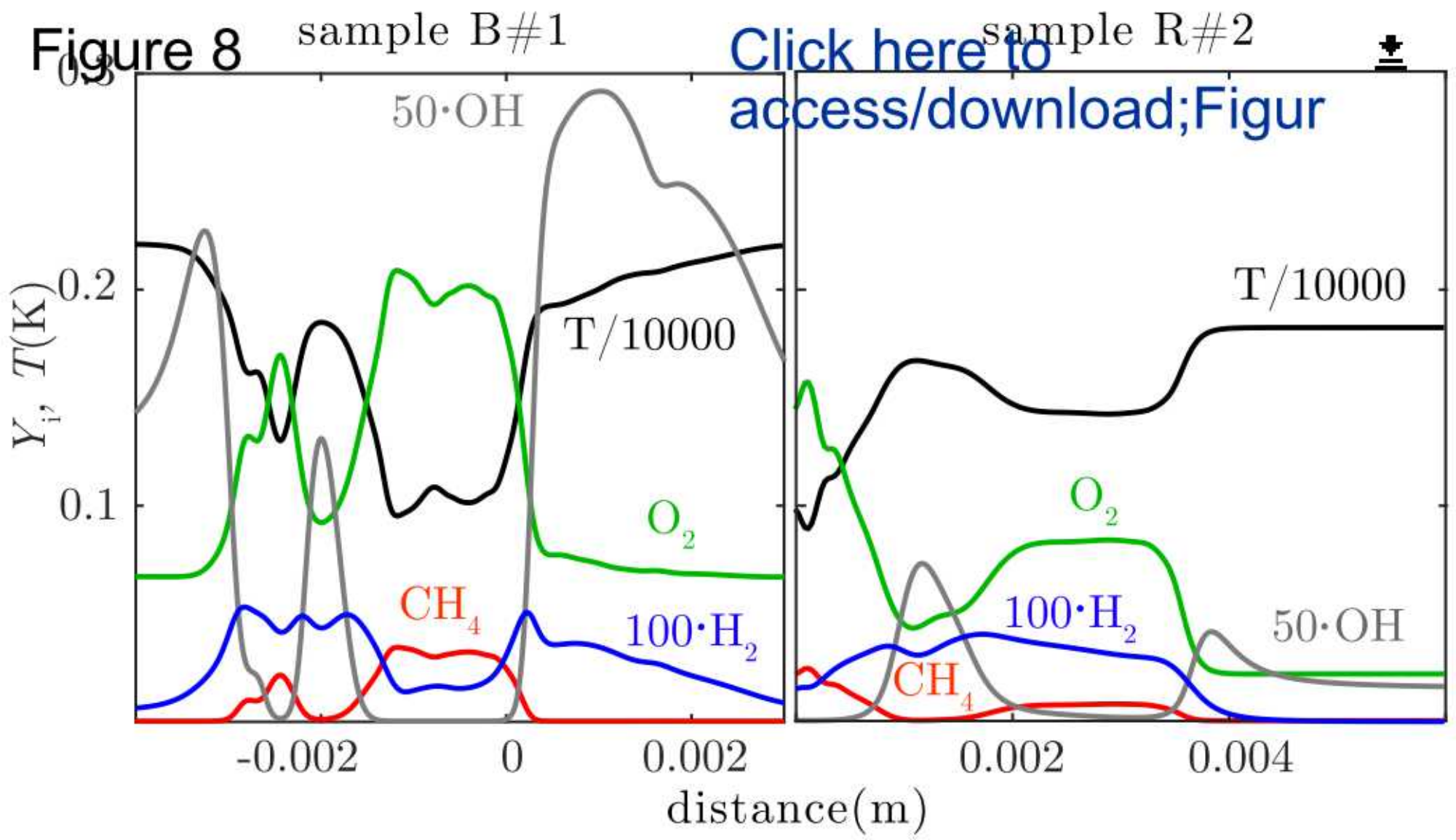

Click here to access/download;Figur

Figure 9

Click here to access/download;Figure;Fig9_SlotUQ_1.

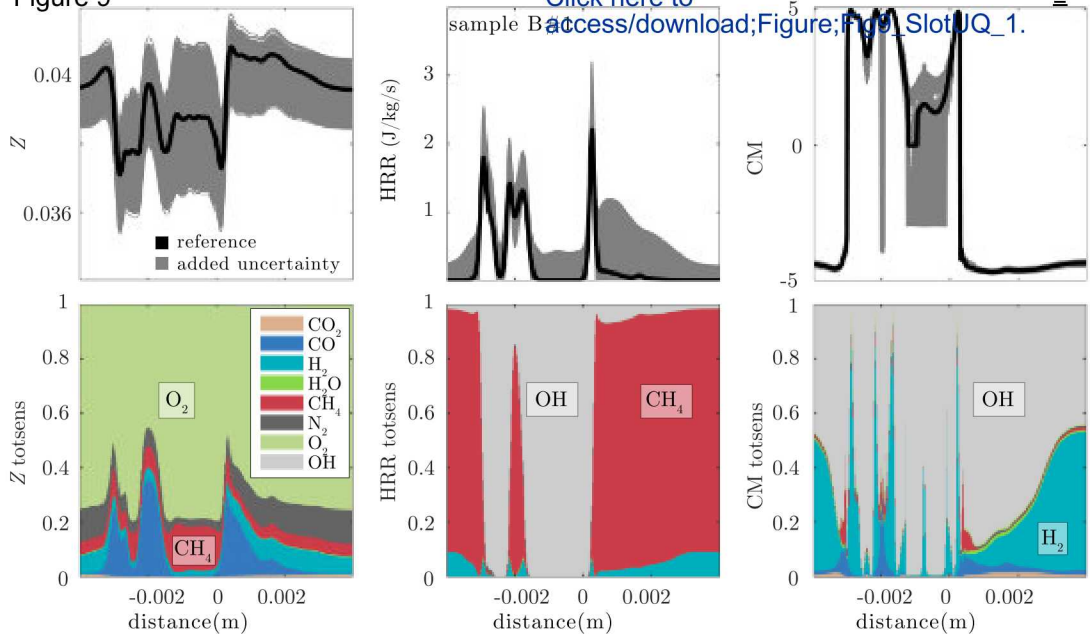

Figure 10

Click here to access/download;Figure;Fig10_LundUQ_

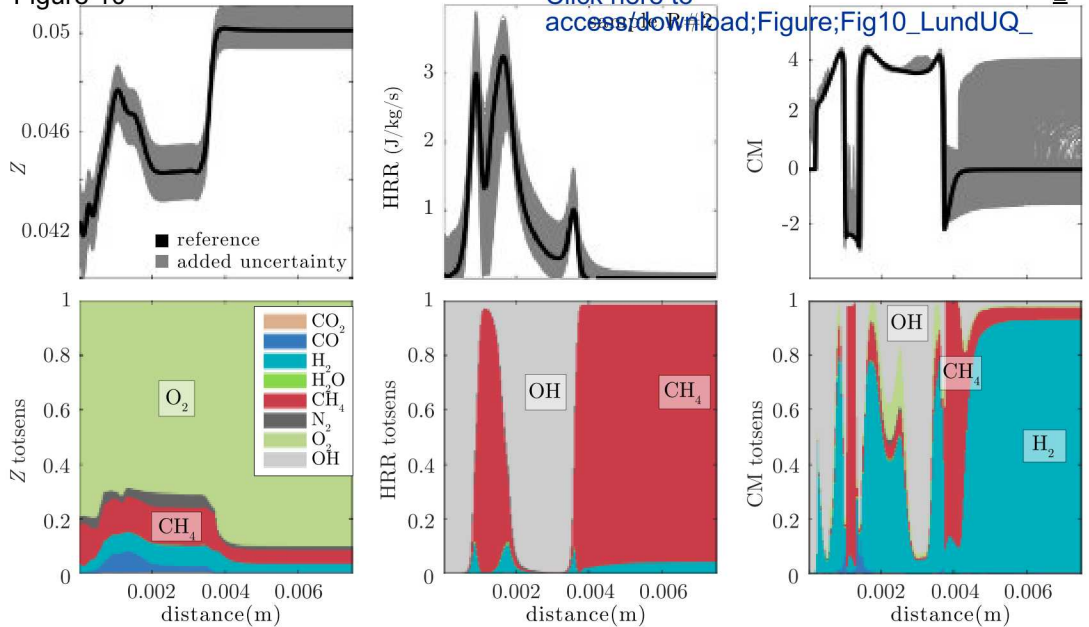

Figure 11

Click here to access/download;Figure;Fig11_BurnerLundSingle.